



HAL
open science

SIMULATION OF CONVECTIVE MASS TRANSFER IN A NEAR-CRITICAL BINARY MIXTURE ABOVE AN ADSORBENT BOUNDARY

Smahi Housseynes, Djilali Ameer, Joanna Dib, Isabelle Raspo

► **To cite this version:**

Smahi Housseynes, Djilali Ameer, Joanna Dib, Isabelle Raspo. SIMULATION OF CONVECTIVE MASS TRANSFER IN A NEAR-CRITICAL BINARY MIXTURE ABOVE AN ADSORBENT BOUNDARY. 4th Conference on Energy, Materials, Applied Energetics and Pollution (ICE-MAEP2018), Apr 2018, Constantine, Algeria. hal-02117710

HAL Id: hal-02117710

<https://amu.hal.science/hal-02117710>

Submitted on 2 May 2019

HAL is a multi-disciplinary open access archive for the deposit and dissemination of scientific research documents, whether they are published or not. The documents may come from teaching and research institutions in France or abroad, or from public or private research centers.

L'archive ouverte pluridisciplinaire **HAL**, est destinée au dépôt et à la diffusion de documents scientifiques de niveau recherche, publiés ou non, émanant des établissements d'enseignement et de recherche français ou étrangers, des laboratoires publics ou privés.

SIMULATION OF CONVECTIVE MASS TRANSFER IN A NEAR-CRITICAL BINARY MIXTURE ABOVE AN ADSORBENT BOUNDARY

Smahi Housseyn¹, Djilali Ameer², Joanna Dib³, Isabelle Raspo⁴

¹Laboratory of Theoretical Physics, Faculty of Sciences, University of Tlemcen, Algeria, housseynsmahi@gmail.com

²Laboratory of Theoretical Physics, Faculty of Sciences, University of Tlemcen, Algeria, d.ameur@yahoo.fr

³Laboratory of Theoretical Physics, Faculty of Sciences, University of Tlemcen, Algeria, joannadib2022@yahoo.fr

⁴Aix-Marseille Université, CNRS, Centrale Marseille, M2P2 UMR7340, Marseille, France, isabelle.raspo@univ-amu.fr

ABSTRACT

In this work, we present a study of the adsorption for dilute solute (Naphthalene) in supercritical CO₂ enclosed in a rectangular cavity. The effect of proximity to the critical point on mass transfer is numerically investigated. The numerical model is based on the resolution of the Navier-Stokes equations coupled with the energy and mass diffusion balances. The velocity field, the mass fraction perturbation as well as the temporal evolution of the mean Sherwood number is presented for various temperatures. The results show that close to the mixture critical point, the homogeneous adsorption of the solute is obtained. Additional key findings include that closer we get to the critical point, the better is the mass transfer on the adsorbent plate.

Key words: *Mass transfer, Adsorption, Supercritical carbon dioxide (scCO₂), mixture fluid, Piston effect*

GLOSSARY

Symbols:

P Pressure, Pa
T temperature, K
V velocity, m/s
Re Reynolds number
C_v heat capacity, J.kg⁻¹.K⁻¹
Fr Froude number
Ra Rayleigh number
ω mass fraction
H characteristic height, mm
L cavity length, mm
Ma Mach number
Pr Prandtl number
Le Lewis number
R perfect gas constant, J/kg.K
Sh Sherwood number
t time, s
u velocity component in the x direction, m/s
PE piston effect

v velocity component in the y direction, m/s
x cartesian axis direction, mm
D₂₁ binary mass diffusion coefficient, m²/s

Greek letters:

ρ density, kg.m⁻³
ε dimensionless proximity to the critical point
μ dynamic viscosity, Pas
δt dimensionless time step, s
β thermal expansion coefficient, K⁻¹
γ ratio of heat capacities
λ thermal conductivity, W.m⁻¹.K⁻¹

Indices / Exhibitors:

c critical property
i initial value
th thermodynamic part
h heat
(* dimensionless parameters)

1. INTRODUCTION

The supercritical fluid (SCF) is a fluid for which temperature and pressure are larger than those of the critical point. In this zone of the phase diagram, the physical properties of the fluid (density, viscosity, diffusivity) are intermediate between those of liquids and gases [1, 2]. Supercritical fluid deposition (SFD) is a promising technique aiming to prepare supported metallic nanoparticles or metallic films and has been the subject of several researchs and publications [3, 4, 5]. In this technique, supercritical CO₂ (scCO₂) has been used in most of the depositions because it is non-flammable and non-toxic. Using supercritical fluids (SCFs) to deposit metals and metaloxides on surfaces has been attracting due to the attractive properties of supercritical fluids. Supercritical fluid deposition (SFD) in particular using supercritical carbon dioxide (scCO₂) is attractive because no liquid the waste is generated, no solvent residue is left on the substrate and the mass transfer rates are fast compared to the liquids [4]. In addition, the rate and the velocity of the substrate deposition can be controlled by the changing of the pressure and temperature of solvent presented here by the supercritical carbon dioxide (scCO₂). In this paper, Naphthalene was chosen as a model solute because its phase equilibria with CO₂ has been thoroughly studied [3, 6, 7]. There are extensive data available for this system that have been confirmed.

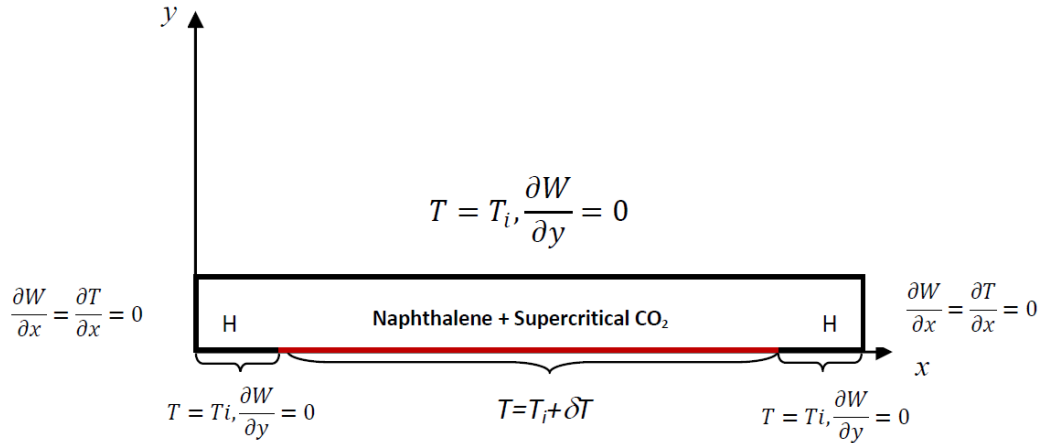


FIGURE 1 Physical configuration

The physical model consists of a dilute solute (Naphthalene-scCO₂) mixture enclosed in a rectangular cavity with a heated and adsorbent plate on the bottom boundary so showed in figure 1 of height $H=1\text{mm}$. An adiabatic boundary condition was applied to the non-reactive vertical and upper walls. Its temperatures are maintained fixed to T_i . The fluid is considered in thermodynamic equilibrium at a constant temperature T_i slightly above a particular mixture critical temperature $T_{cm} = 307.65\text{ K}$ and $T_i = (1 + \epsilon)$, where $\epsilon = (T_i - T_{cm}) / T_{cm}$ defines the dimensionless proximity to the critical point. The critical property T_{cm} corresponds to the Lower Critical EndPoint of the mixture and is slightly above the critical point of CO₂. A weak gradually heating is then applied at the solid bottom plate ($y = 0$ for $H < x < L - H$).

2. MATHEMATICAL MODEL

The mathematical model is based on the 2D time-dependent and compressible Navier–Stokes equations, coupled with energy and mass diffusion equations including the supplemental Peng–Robinson equation of state. In order to reduce computational costs, these equations are solved in the framework of the low Mach number approximation [8]. Thus, the total pressure is split into two parts: a homogeneous thermodynamic part $P_{th}(t)$, which appears in the equation of state and in the energy equation and only depends on time t , and a non-

homogeneous dynamic part $P_{\text{dyn}}(x, y, t)$, appearing in the momentum equation and which varies with time and space. The dimensionless governing equations are therefore:

$$\rho \frac{\partial \rho}{\partial t} + \frac{\partial}{\partial x}(\rho V) = 0 \quad (1)$$

$$\rho \frac{\partial V}{\partial t} + \rho V \cdot \nabla V = -\nabla P_{\text{dyn}} + \frac{1}{Re} \Delta V + \frac{1}{3Re} \nabla(\nabla \cdot V) + \frac{1}{Fr} \rho \quad (2)$$

$$\rho \frac{\partial T}{\partial t} + \rho V \cdot \Delta T = -\frac{C_{V0}}{C_{Vi}} (\gamma_0 - 1) \left[P_{th} - T \left(\frac{\partial P_{th}}{\partial T} \right)_{\rho, \omega} \right] (\nabla \cdot V) + \frac{\gamma}{Re Pr} \nabla \cdot (\lambda^* \nabla T) - \left[(\bar{U}_2^* - \bar{U}_1^*) + \frac{C_{V0}}{C_{Vi}} (\gamma_0 - 1) \times \left(P_{th} - T \left(\frac{\partial P_{th}}{\partial T} \right)_{\rho, \omega} \right) (\bar{V}_2^* - \bar{V}_1^*) \right] \times \frac{1}{(\gamma-1)^2 Le \theta(\omega)} \nabla \cdot (\rho D_{21}^* \nabla \omega) \quad (3)$$

$$\rho \frac{\partial \omega}{\partial t} + \rho V \cdot \nabla \omega = \frac{1}{(\gamma-1)^2 Le} \nabla \cdot (\rho D_{21}^* \nabla \omega) \quad (4)$$

V is the velocity of components u and v in the x - and y -directions respectively, w is the mass fraction, γ is the ratio of the isobaric and isochoric specific heats calculated from the equation of state with γ_0 and C_{V0} corresponding to the values for a perfect gas ($\gamma_0 = 1.3$, $C_{V0} = 3R/M_1$). The dimensionless numbers are respectively, the Mach number Ma , the Reynolds number Re , the Froude number Fr , the Prandtl number Pr and the Lewis number Le and are defined as:

$$Ma = \frac{V_{PE}}{C_0} \quad ; \quad Re = \frac{\rho_i V_{PE} H}{\mu_i} \quad ; \quad Fr = \frac{V_{PE}^2}{gH} \quad ; \quad Pr = \frac{\mu_i \gamma C_{Vi}}{\lambda_i} \quad ; \quad Le = \frac{\lambda_i}{\rho_i \gamma C_{Vi} (D_{21})_i}$$

where $C_0 = \sqrt{\gamma_0 \left(\frac{R}{M} \right) T_{cm}}$ is the sound speed and $V_{PE} = H/t_i$ is the characteristic velocity of the piston effect [6, 7, 9]. It must be noted that the divergence of the infinite-dilution properties of the solute is not specific of Naphthalene but it is a universal behavior for dilute mixtures [3].

3. RESULTS

Simulations were performed for a heating $\Delta T = 10\text{mK}$ and three initial temperatures $T_i = 308.15\text{K}$, 309.15K and 318.15K , which correspond to distances to the mixture critical point equal to 0.5K , 1.5K and 10.5K respectively. The mixture is saturated, which means that the initial mass fraction w_i corresponds to the solubility of Naphthalene in CO_2 . The values of the various properties and transport coefficients at the initial states considered are given in Table 1. As already said in section 2, since the binary mixture is very dilute because of the low solubility of the solute, we can assume that the transport coefficients of the mixture are those of the pure solvent. Thus, the thermal expansion coefficient β and the ratio of heat capacities γ were calculated from the Peng-Robinson equation for pure CO_2 .

| T_i | w_i | μ_i | λ_i | C_{Vi} | $(D_{21})_i$ | β_i | γ |
|--------|-------------------------|-------------------------|-------------------------|----------|-------------------------|-------------------------|----------|
| 308.15 | 7.6751×10^{-3} | 3.3402×10^{-5} | 9.6172×10^{-2} | 1306.27 | 2.1969×10^{-8} | 2.3134×10^{-1} | 16.75 |
| 309.15 | 8.0713×10^{-3} | 3.3448×10^{-5} | 9.1322×10^{-2} | 1269.32 | 2.2009×10^{-8} | 1.7465×10^{-1} | 13.95 |
| 318.15 | 1.2557×10^{-2} | 3.3870×10^{-5} | 6.6804×10^{-2} | 1074.57 | 2.2368×10^{-8} | 5.4955×10^{-2} | 6.51 |

TABLE 1. Initial values of temperature, mass fraction and transport coefficients.

The Damköhler number was fixed to $Da=10^{-5}$, which is a pertinent value for an adsorption reaction. Figure 2 shows the isolines of temperature and mass fraction perturbation at two times for the three initial temperatures. The first time corresponds to $2.5t_{PE}$ for all the cases. The solutions obtained for the various values of T_i are similar. The temperature field at this time is governed by the Piston effect, as in pure CO_2 [10], with three distinct zones: a hot boundary layer along the heated plate, cold boundary layers along isothermal walls and the cavity bulk which is homogeneously heated by the Piston effect. In addition, as in pure CO_2 , the thermal boundary layers are thinner when approaching the critical point because of the strong decrease of thermal diffusion.

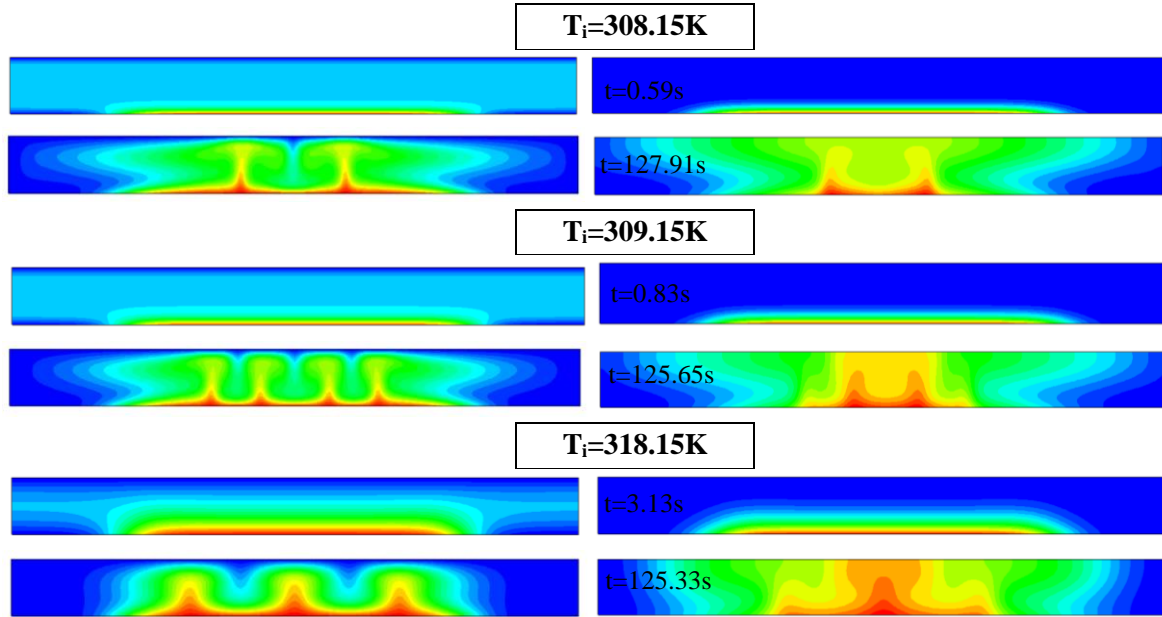


FIGURE 2. Isolines of temperature (left column) and mass fraction perturbation $w-w_i$ (right column) for the three initial temperatures.

In the same way, the isolines of the mass fraction perturbation reveal the existence, along the adsorbent plate, of a thin boundary layer which becomes thinner when approaching the critical point because of the decrease of the mass diffusion coefficient D_{21} (Table 1). Figure 2 also presents the steady solution obtained for each initial temperature. Concerning the mass fraction, it must be underlined that, although the isoline map does not evolve anymore, the values of $w-w_i$ keeps on increasing while the adsorption reaction still goes on. As expected, the temperature field is very different depending on the proximity to the critical point. Indeed, because of the diverging behavior of the thermal expansion coefficient β (Table 1), the Rayleigh number strongly increases as approaching the critical temperature: $Ra=3683$ for $T_i=318.15K$, $Ra=21938$ for $T_i=309.15K$ and $Ra=34139$ for $T_i=308.15K$. As a consequence, the convective flow is much more intense for $T_i=308.15K$ (Fig. 3.(a)), allowing a better mixing inside the cavity. The distribution of the convection cells directly affects the mass fraction field as it is revealed in figure 3 showing the velocity field together with the isolines of $w-w_i$. The jet flow between contrarotative rolls is much weaker for $T_i=318.15K$ (Fig. 3.(b)) allowing the development of a high mass fraction “plume” rising at the middle of the heated plate (Fig. 2). For $T_i=308.15K$, in contrast, the very intense convection flow restricts the diffusion of the solute in the boundary layer along the plate. The mass fraction field obtained for $T_i=309.15K$ is intermediate between those previously described (Fig. 2).

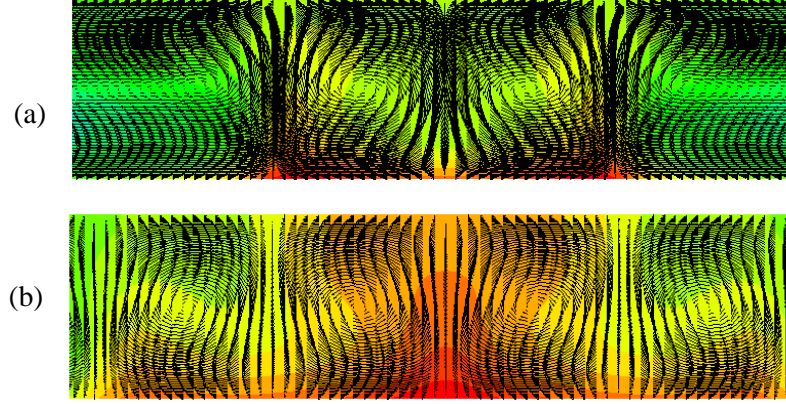


FIGURE 3. Velocity field together with the isolines of $w-w_i$ in the central part of the cavity (above the heated plate) for (a) $T_i=308.15\text{K}$ and (b) $T_i=318.15\text{K}$.

The convection flow has also a strong influence on the adsorbed amount of solute. Figure 4 presents the profile of the relative mass fraction perturbation $(w-w_i)/w_i$ on the bottom boundary for the three initial temperatures. Although the maximum amount adsorbed on the plate increases when moving away from the critical point, the profiles reveal that the adsorption of the solute is strongly inhomogeneous for $T_i=318.15\text{K}$, with a peak of adsorption in the middle of the plate. On the other hand, close to the critical point ($T_i=308.15\text{K}$), the peak at $x=L/2$ is less pronounced, leading to a more homogeneous adsorption of the solute and, therefore, a more homogeneous material in the framework of SFD processes for example.

Finally, the effect of the proximity to the critical point on the mass transfer at the adsorbent plate was considered. For this purpose, we calculated the mean Sherwood number on the plate. This dimensionless number, which characterizes the mass transfer at a boundary, is defined by:

$$Sh = - \int_{plate} \frac{H}{(D_{21})_i (w(x, 0, t) - w(x, \frac{H}{2}, t))} D_{21} \frac{\partial w}{\partial y} dx$$

Figure 5 shows the temporal evolution of the Sherwood number for the three initial temperatures. A Strong value of Sh is observed at the very beginning of the simulations because of the increase of the plate temperature from T_i to $T_i+\Delta T$. Then the Sherwood number rapidly decreases to reach its steady state value. The drop observed between around 5s and 10s is due to the impact of a large cold thermal plume on the heated plate. Figure 5 reveals that the Sherwood number in the steady solution strongly increases when approaching the critical point, with a value of Sh about 1.5 times larger at $T_i=308.15\text{K}$ than the one at $T_i=318.15\text{K}$. In other words, getting closer to the mixture critical point enables a better mass transfer at the adsorbent plate.

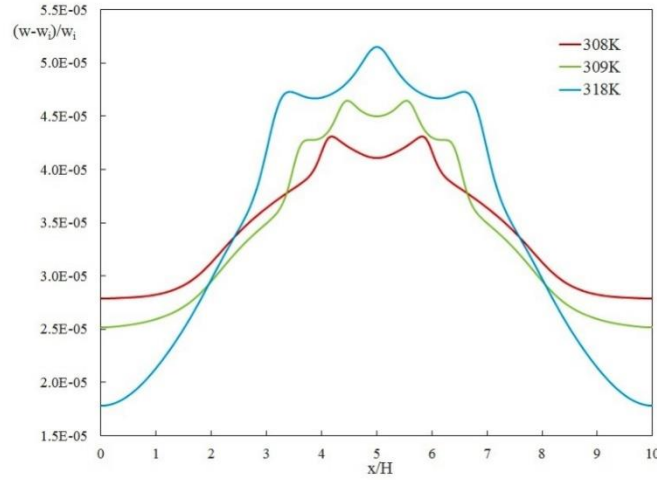


FIGURE4. Profiles of the relative mass fraction perturbation on the bottom boundary for the three initial temperatures.

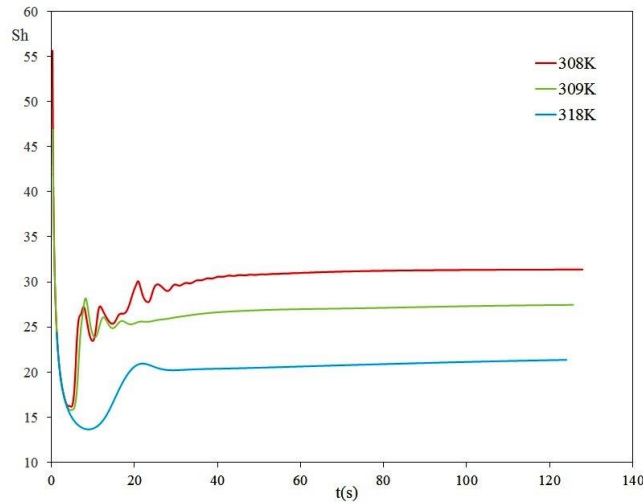


FIGURE5. Temporal evolution of the mean Sherwood number for the three initial temperatures.

4. CONCLUSIONS

In this paper, we presented a numerical study of heat and mass transfer in a dilute near-critical binary mixture enclosed in a rectangular cavity with a heated and adsorbent plate on the bottom boundary. The Naphthalene-CO₂ mixture was chosen as a model mixture because of the substantial experimental data on solubility of Naphthalene, allowing a correct determination of binary parameters in the mixing rules of the equation of state. However, since the diverging behaviors of transport coefficients near critical points are universal, we believe that the conclusions of our study could be applied to any binary mixture exhibiting the same kind of phase diagram. The results showed that, because of the divergence of the thermal expansion coefficient, a more homogeneous adsorption profile can be obtained for a same value of the heating when moving closer to the mixture critical point. In addition, approaching the critical point also leads to a better mass transfer at the adsorbent plate. These two phenomena can be of great interest for SFD processes.

REFERENCES

- [1] D. Ameer, I. Raspo, Numerical simulation of the Poiseuille-Rayleigh-Bénard instability for a supercritical fluid in a mini-channel, *Comput. Thermal Sci.* 5, pp. 107–118, 2013.
- [2] D. Ameer, I. Raspo, J. Dib, Thermoconvective instabilities of 2D Poiseuilles-Rayleigh-Benard for supercritical fluids in micro/macro-channels, Proceedings of the 1st Thermal and Fluid Engineering Summer Conference, TFESC, August 9-12, 2015, New York City, USA.
- [3] M. Wannassi, I. Raspo, Numerical study of non-isothermal adsorption of Naphthalenein supercritical CO₂: Behavior near critical point, *J. of Supercritical Fluids* 117, 203–218, 2016
- [4] C. Erkey, Preparation of metallic supported nanoparticles and films using supercritical fluid deposition, *J. of Supercritical Fluids* 47, 517-522, 2009
- [5] S.E. Bozbag and C. Erkey, Supercritical deposition: Current status and perspectivesfor the preparation of supported metal nanostructures, *J. of Supercritical Fluids* 96, 298–312, 2015
- [6] I. Raspo, S. Meradji, B. Zappoli, Heterogeneous reaction induced by the piston effect in supercritical binary mixtures, *Chem. Eng. Sci.* 62, 4182–4192, 2007.
- [7] I. Raspo, B. Zappoli, P. Bontoux, Fast mass transfer at a solid–supercritical fluid interface by piston effect, in: *Proceedings of 4th ICCHMT*, May 17–20, Paris-Cachan, 2005.
- [8] S. Paolucci, On the filtering of sound from the Navier-Stokes equations. *Technical report, Sandia National Laboratories, USA, (SAND82-8257)*, 1982.
- [9] G. Accary, I. Raspo, P. Bontoux, B. Zappoli, An adaptation of the low Mach number approximation for supercritical fluid buoyant flows, *C. R. Mec.* 331, 397–404, 2005.
- [10] S. Amiroudine, P. Bontoux, P. Larroudé, B. Gilly and B. Zappoli, Direct numerical simulation of instabilities in a two-dimensional near-critical fluid layer heated from below, *Journal of Fluid Mechanics*, 442, 119-140, 2001.